9-21-2023

High-Sensitivity Electronic Stark Spectrometer Featuring a Laser-Driven Light Source

J. S. Huff
Boise State University

K. M. Duncan
Boise State University

C. J. Van Galen
Temple University

M. S. Barclay
Boise State University

W. B. Knowlton
Boise State University

See next page for additional authors

Review of Scientific Instruments ARTICLE pubs.aip.org/aip/rsi

High-sensitivity electronic Stark spectrometer featuring a laser-driven light source

Cite as: Rev. Sci. Instrum. 94, 094103 (2023); doi: 10.1063/5.0153428
Submitted: 7 April 2023 • Accepted: 21 August 2023 •
Published Online: 20 September 2023

J. S. Huff,[1] K. M. Duncan,[1] C. J. van Galen,[2] M. S. Barclay,[1] W. B. Knowlton,[1,3] B. Yurke,[1,3] P. H. Davis,[1,4] D. B. Turner,[1,a)] R. J. Stanley,[2] and R. D. Pensack[1,b)]

AFFILIATIONS

[1] Micron School of Materials Science and Engineering, Boise State University, Boise, Idaho 83725, USA
[2] Department of Chemistry, Temple University, Philadelphia, Pennsylvania 19122, USA
[3] Department of Electrical and Computer Engineering, Boise State University, Boise, Idaho 83725, USA
[4] Center for Advanced Energy Studies, Idaho Falls, Idaho 83401, USA

[a)] Electronic mail: danielturner926@boisestate.edu
[b)] Author to whom correspondence should be addressed: ryanpensack@boisestate.edu

ABSTRACT

We report developmental details of a high-sensitivity Stark absorption spectrometer featuring a laser-driven light source. The light source exhibits intensity fluctuations of ~0.3% over timescales ranging from 1 min to 12 h, minimal drift (≤0.1%/h), and very little $1/f$ noise at frequencies greater than 200 Hz, which are comparable to or better than an arc-driven light source. Additional features of the spectrometer include balanced detection with multiplex sampling, which yielded lower noise in A, and constant wavelength or wavenumber (energy) spectral bandpass modes. We achieve noise amplitudes of ~7×10^{-4} and ~6×10^{-6} in measurements of single A and ΔA spectra (with 92 data points) taking ~7 and ~19 min, respectively.

I. INTRODUCTION

Stark absorption (or electroabsorption) spectroscopy is a powerful method used to obtain the difference dipole moment (Δd), i.e., extent of charge transfer with light absorption, of a chromophore along with the angle (ζ) between Δd and the transition dipole moment (μ). In the visible region of the electromagnetic spectrum, additional details such as change in polarizability ($\Delta\alpha$) can be obtained. However, the measured Stark signal is small—generally of the order 10^{-3} to 10^{-6}—and requires specialized instrumentation. Many excellent articles,[1–4] reviews,[5–8] and book chapters[9–11] have been dedicated to the topic, which also include details for non-specialists.

The most common light source for Stark spectroscopy is an arc-driven xenon lamp, which is bright (i.e., intense) over a broad spectral range (typically ~250 to 2500 nm). However, the output of an arc-driven xenon lamp has been shown to have considerable short-timescale fluctuations and long-timescale drift.[12–14] Recently, a laser-driven xenon lamp, which we will hereafter refer to as a laser-driven light source (LDLS), has emerged as an alternative.[15] In an LDLS, a laser maintains the plasma in the lamp even after initial electrical arcing. As a result, an LDLS is potentially more stable and exhibits an improved spatial mode. To date, it has been successfully implemented in a number of spectrometers, including Stark spectrometers for measurements of thin films[16,17] and in a transient absorption spectrometer for measurements of solutions.[18] Although the latter work reported many details of the LDLS itself, including low-intensity fluctuations, estimated to be ~0.2%, the performance of an LDLS and an arc-driven xenon lamp have not been compared to the best of our knowledge.

Here, we report developmental details of a high-sensitivity, electronic Stark spectrometer (ESS) featuring an LDLS. In addition to the LDLS, other notable features of the ESS include a reference detector for balanced detection, along with an 18-bit data acquisition (DAQ) board for multiplex sampling. Finally, the ESS features a monochromator that enables measurements with either constant wavelength or wavenumber (energy) spectral bandpass.

II. METHODS

Figure 1 displays a schematic of the high-sensitivity ESS. The ESS features a laser-driven xenon source (Energetiq, EQ-99X),

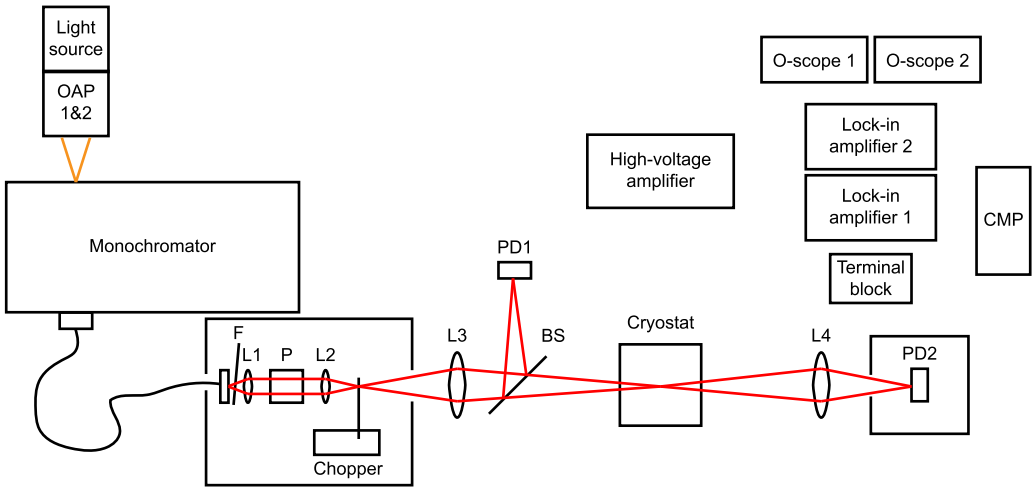

FIG. 1. Schematic of the electronic Stark spectrometer, emphasizing the optical layout. Orange and red lines, intended to depict polychromatic and monochromatic light, respectively, highlight the optical path. F is a 515-nm, long-pass filter. L1 and L2 are 1 in. diameter f = 25 mm and f = 50 mm biconvex lenses, respectively. P is a Glan-Laser polarizer. L3 and L4 are 2 in. diameter f = 100 mm and f = 60 mm biconvex lenses, respectively. BS is a reflective neutral density filter, serving as a beamsplitter. PD1 and PD2 are silicon-based photoreceivers. The sample capacitor is situated in a modified, dual-chamber liquid nitrogen optical cryostat. The PD1 and PD2 signals are sent to a terminal block, which transfers these signals to a DAQ card connected to a computer (labeled CMP). Additional details of the detection electronics, triggering scheme, and high-voltage electronics, such as the sample rod and components, are included in Appendix B. The optical chopper and PD2 are enclosed in a blackout box and a combined blackout box/Faraday cage, respectively.

which was purged with high-purity (99.999%) nitrogen gas at a rate of 0.5 L/min. The output of the LDLS is collimated and focused with a pair of off-axis, parabolic (OAP) mirrors, with effective focal lengths of 2 and 6 in., respectively. The light is focused onto the entrance slit of a monochromator with an f/# of 3.9 (Spectral Products, DK240). The monochromator features a 1200 g/mm diffraction grating blazed at 500 nm. In constant wavelength bandpass measurements, both entrance and exit slit widths are set to 500 μm, which, given an angle of 18.5° between the incident and diffracted beams in the monochromator, result in a spectral bandpass of ~3.4 nm or ~30 to 130 cm^{-1} over the usable range of the instrument (i.e., ~515 to 1030 nm).[19] A fiber-optic adapter (Spectral Products, AF-DK-L) situated after the exit slit uses a UV fused silica (FS) lens to focus the light into an optical fiber with a 400 μm core that is 1 m long and transparent from 250 to 1150 nm (Spectral Products, SF0400-SMSM-U10). The purpose of the fiber is to randomize the light polarization and improve the spatial mode for subsequent use in the spectrometer.[11] A long-pass filter (Thorlabs, FGL515) is situated at the output of the fiber to reject high-order diffraction of short wavelength light. A 1 in. diameter f = 25 mm lens (L1) collimates the beam to a width of about 13 mm, which then propagates through a Glan-Laser polarizer (P) with a 15 mm diameter clear aperture (Thorlabs, GL15). A 1 in. diameter f = 50 mm lens (L2) focuses the light to a width of ~1 to 2 mm, where the slotted wheel of an optical chopper (Newport, 3502) is situated. A 2 in. diameter f = 100 mm lens (L3) is located ~200 mm past the focus, such that the beam is magnified. After L3, a beamsplitter (Thorlabs, NDUV2R10A) sends a portion of the light to a "reference" detector (Femto, OE-200-SI), and the remainder of the light is focused to the sample position, where the sample capacitor is immersed in liquid nitrogen (Janis, modified dual-immersion VPF-100) and oriented at 45° with respect to the incident beam. After passing through the sample, a 2 in. diameter f = 60 mm lens (L4) is situated ~180 mm away to focus the light onto a "signal" detector (Femto, OE-200-SI). L1 and L2 are composed of UV FS, while L3 and L4 are composed of N-BK7 and UV FS, respectively; all lenses are biconvex. The chopper and PD2 are enclosed by black corrugated plastic, held in place with black structural rails; the latter enclosure is also lined with copper mesh with 1.4 mm spacing to form a Faraday cage.

For absorption measurements, where $A = -\log(I/I_0)$, I and I_0 are collected in two separate scans over wavelength (or energy) to produce a single measured spectrum. To facilitate measuring the signal, the light-source intensity is modulated on and off at 1000 Hz with the optical chopper. The outputs of the signal and reference detectors are sent to dual- and single-phase lock-in amplifiers (LIAs), respectively (Stanford Research Systems, SR830 and SR810). A TTL pulse is generated by the dual-phase LIA, which is used as the reference/trigger source for the optical chopper, single-phase LIA, and an 18-bit DAQ board (NI, PCI-6281). The time constant and sensitivity of both LIAs are set to 100 ms and 1 V, respectively. Neutral density filters (Thorlabs, NUK01) situated in front of PD1 and PD2 are selected to maximize the largest signal in the spectral region of interest (typically ~824.5 or 883.5 nm) without saturating the LIA inputs. Iris diaphragms and lens tubes are attached to the front of PD1 and PD2 to suppress ambient light. The DAQ board digitizes the signals output by the two LIAs. For reasons noted in Appendix A, passive, 10 kHz low-pass filters are placed between the detectors and the DAQ board. The PD and LIA outputs are terminated at 1 MΩ at two different oscilloscopes (Keysight, DSOX3014T and Agilent, DSO5014A, respectively). I (I_0) and I_{ref} ($I_{0,ref}$) are sampled 100 times at 200 Hz in a multiplexed manner.

I/I_{ref} and $I_0/I_{0,ref}$ are calculated for each pair of samples, and the 100 results are averaged.

For Stark absorption measurements, where $\Delta A \approx \Delta I/I$, ΔI and I are collected in a single scan to produce a single measured spectrum. To generate the signal, the optical response of the sample is modulated by an applied electric field. Specifically, the dual-phase LIA generates a pure sine wave that is sent to a 1000 V/V high-voltage amplifier (Trek, 609E-6). The high-voltage waveform is then transmitted across a capacitor that includes a sample with a Stark response. A neutral density filter in front of PD2 is chosen to maximize its output voltage in the spectral region of interest. To measure I, the output of PD2 is measured directly via the DAQ board. The output of PD2 is then sent to the input of the dual-phase LIA, which is set to detect the Stark signal at twice the applied field frequency. The time constant of the LIA is set to 1 s, and its sensitivity is set to optimize the dynamic range, while also staying below saturation. The LIA's auto phase function is used to set the correct phase, thereby maximizing the Stark signal. As above, the DAQ board digitizes the output of the dual-phase LIA, which is converted to ΔI. Given that the microprocessor of the dual-phase LIA is 16-bit, negligible noise is added by the 18-bit DAQ board. I and ΔI are sampled 50 000 times at 100 kHz in a multiplexed manner. ΔA is calculated as $1/\ln(10) \times -\Delta I/I$ for each of the 50 000 sample pairs, which are then averaged.

In A (ΔA) measurements, the LIA low-pass filter slope is set to 6 (24) dB/oct, and the signals are detected after allowing the LIAs to settle for 5 (10) time constants. All signals are transmitted with double-shielded, RG142 coax cables (Pasternack, PE3495). The computer, including the DAQ board attached via a PCI port, has a CPU featuring four cores with a base frequency of 3.60 GHz (Intel, Core i7-7700) and 32 GB of RAM. Custom software (National Instruments, LabVIEW 2020) was written to automate hardware motion and data acquisition.

Additional details of the detection electronics, triggering scheme, and applied field electronics, such as the sample rod and components, are included in Appendix B.

III. RESULTS AND DISCUSSION

The LDLS exhibits good stability. Figure 2 displays the light intensity characterization. Panel a shows that over the course of an hour, the relative standard deviation (RSD) is 0.32 ± 0.02%, with an average long-term drift of 0.1 ± 0.1%/h. Three independent scans were measured at 850 nm and found to be largely identical (for the spectrum of the LDLS in the ESS, see the inset of panel a). We note that an even smaller RSD of 0.092 ± 0.005% was attainable without nitrogen gas purging. From additional scans conducted at ten wavelengths spanning 520–1000 nm, we determined that the intensity fluctuations are largely independent of wavelength, with RSD values ranging from 0.2% to 0.3%. Critically, we measure the same RSD over the course of 7 and 19 min, which is the time required to make single A or ΔA measurements, respectively. Remarkably, nearly equivalent results are observed in a 12 h scan; specifically, the LDLS intensity exhibits an RSD of ~0.3% with long-term drift of less than 0.1%/h. We also simultaneously measured the laboratory room temperature and computed the Pearson correlation coefficient between the LDLS intensity and room temperature to be 0.04. This value indicates that there

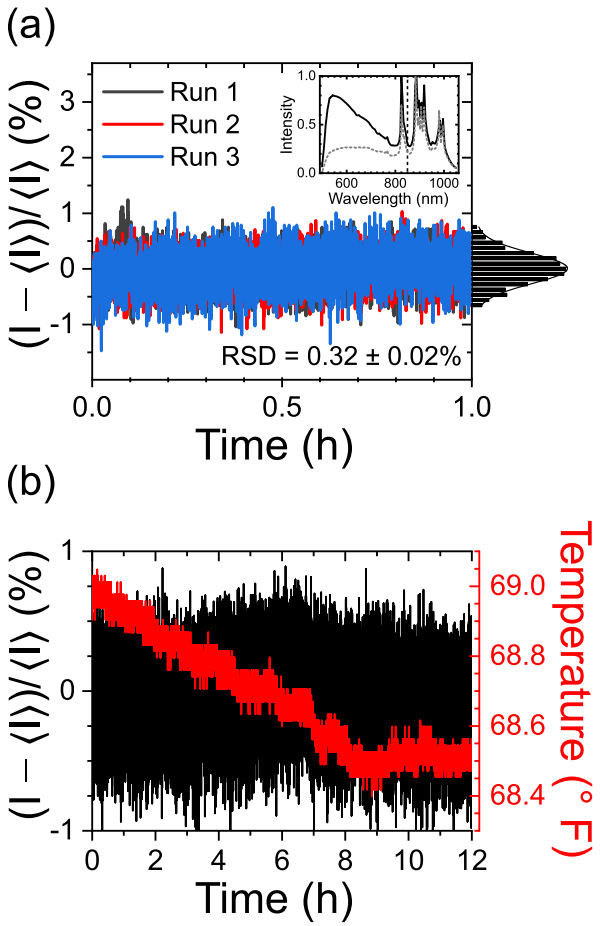

FIG. 2. Light-source intensity fluctuation characterization: (a) short-term fluctuations and (b) long-term fluctuations. A histogram of the fluctuations of the first run is included to the right of the main plot in panel a, with a Gaussian fit overlaid. The inset in panel a displays spectra of the LDLS measured with a constant spectral bandpass of 1.65 nm (black, solid line) and a constant energy bandpass of 30.9 cm^{-1} (gray, dashed line). Light-source intensity measurements were undertaken at 850 nm, which is indicated by the vertical dashed line in the inset. All signals were detected at PD2. Panel b also plots the room temperature measured in parallel with the light intensity.

was effectively no correlation between the light source intensity fluctuations and temperature or that the correlation was below the limit of detection.

In addition to the relatively high stability, the LDLS exhibits very little $1/f$ noise at frequencies at or above 200 Hz. Figure 3 displays Fourier transforms of the light intensity data. Nearly equivalent results are obtained when modulating the intensity by applying a high voltage across the sample; the additional lines appearing at one and two multiples of the applied frequency correspond to an erroneous signal resulting from electromagnetic radiation emitted by the high-voltage amplifier and the Stark signal, respectively. The inset of panel a shows that $1/f$ noise is evident below ~200 Hz, particularly below ~100 Hz. Panel a shows that the noise is constant above 200 Hz. This is a significant advantage of the LDLS over

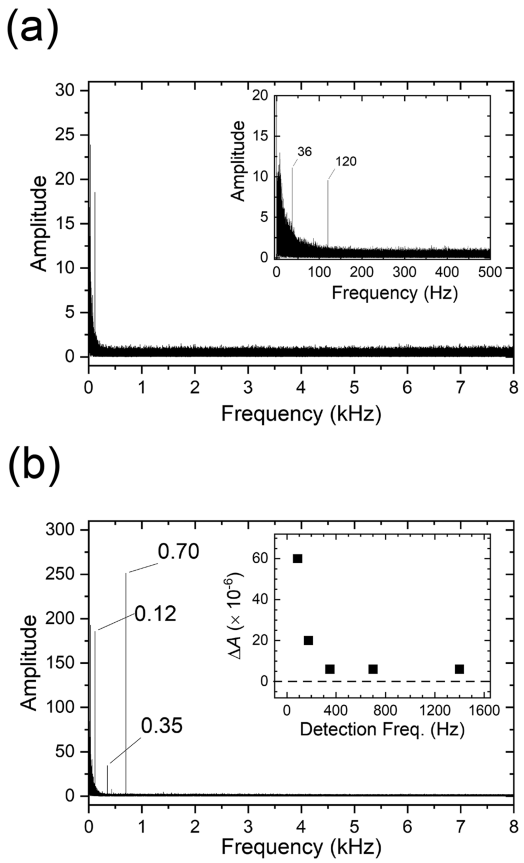

FIG. 3. Fourier transform of the light-source intensity over a frequency range of 8 kHz: (a) in the absence of a sample and applied field and (b) in the presence of a sample and applied field of ~300 kV/cm. The inset of panel a displays a smaller frequency range of 500 Hz in the absence of a sample and applied field. The inset in panel b displays the noise amplitude as a function of detection frequency in a ΔA measurement over the spectral range 805–850 nm.

conventional arc-driven sources because it relaxes constraints on the chopping and applied field frequencies. The inset in panel b shows noise amplitudes measured over the spectral range 805–850 nm as a function of detection frequency in a ΔA measurement. Critically, the noise amplitudes also begin to increase at frequencies below ~200 Hz, and the noise amplitude is the same over the range 350 to 1400 Hz, both observations being consistent with the FFT results. We also characterized an arc-driven xenon lamp featuring a light intensity controller, which exhibited comparable, but slightly poorer performance in RSD, drift, and $1/f$ noise (Appendix C).

At a minimum, both A (i.e., absorption) and ΔA (i.e., Stark absorption) spectra are needed to obtain Δd and $\Delta\alpha$. To obtain ζ, a set of two ΔA spectra can be measured with the light polarization oriented parallel and perpendicular to the applied electric field[11] via the addition of a $\lambda/2$ waveplate. For a sample consisting of a ~240 μM solution of a conjugated asymmetric polymethine molecule (Dyomics, Dy 754), typical signal amplitudes are ~3×10^{-1} and ~7×10^{-4} for A and ΔA, respectively. The capacitor spacing was ~55 μm. The solvent was a 2:1 glycerol:aqueous buffer solution [where the buffer consisted of 1× TAE (i.e., tris base, acetic acid, and ethylenediaminetetraacetic acid) and 15 mM $MgCl_2$ dissolved in water] and the peak molar extinction coefficient of Dy 754 at room temperature was ~163 000 M^{-1} cm^{-1}. Our ESS scheme permits us to consistently achieve noise amplitudes of ~7×10^{-4} and ~6×10^{-6} in A and ΔA measurements, respectively. Noise amplitudes were evaluated as the maximum difference between steps in a spectral region lacking any signal. Thus, we can achieve high signal-to-noise (S/N) ratios of ~430 and ~120, respectively, in a single scan. In some cases, it is either not possible to achieve a sample concentration of 240 μM, or it is desirable to make measurements at a lower concentration to avoid issues such as aggregation. Given the signal and noise amplitudes above, reducing the concentration twelve-fold to 20 μM (and, thus, reducing the signal amplitudes by the same amount) would correspond to a S/N in A and ΔA of ~36 and ~10, respectively, the latter of which can be improved further with signal (ensemble) averaging.[20] For example, averaging five ΔA measurements would result in S/N of ~22 in ~1 h 35 min. Adding a second ΔA measurement with a different light polarization would extend the total acquisition time to ~3 h.

Although the stability of the LDLS is good, it still exhibits short- and long-term fluctuations. In the case of A, where two separate scans (i.e., I and I_0) are collected at different times to produce a single measurement, the observed ~0.3% fluctuations result in noise of the order ~10^{-3}. To overcome this challenge, we implemented balanced detection. In our approach, a reference detector characterizes the LDLS intensity prior to interacting with the sample. In this way, we calculate a corrected A via $-\log([I/I_{ref}]/[I_0/I_{0,ref}])$. Implementing this approach increased the S/N of our A measurements by nearly an order-of-magnitude. Figure 4 shows A spectra calculated with and without correction via balanced detection for a

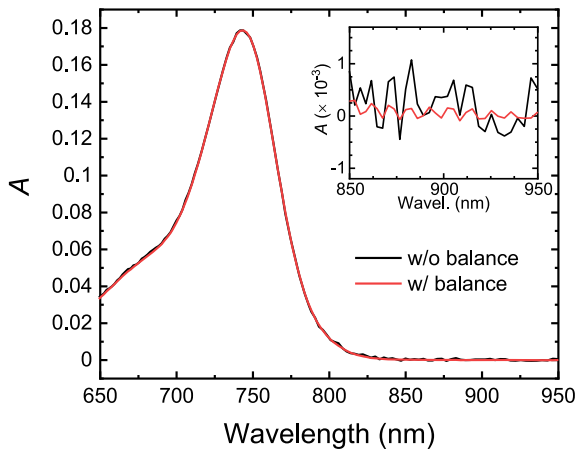

FIG. 4. Spectra acquired via multiplex sampling, with and without balanced detection. These data were collected on a ~5 μM solution of Dy 754 tethered to a DNA Holliday junction, dissolved in an aqueous buffer, and contained in a 2 mm path length cuvette at ~295 K. The data were measured with the incident beam normal to the face of the cuvette. Spectra with and without balanced detection were calculated as $-\log([I/I_{ref}]/[I_0/I_{0,ref}])$ and $-\log(I/I_0)$, respectively. The inset displays a region of the spectrum from 850 to 950 nm, with little to no signal to aid comparison of the respective noise levels.

reference sample in a 2 mm cuvette. Balanced detection reduced noise associated with both short- and long-term fluctuations. In the case of spectra calculated without and with balanced detection, the noise amplitude associated with short-term fluctuations was reduced from 1×10^{-3} to 3×10^{-4}, respectively, as shown in the inset of Fig. 4. Furthermore, baseline offsets and line shape changes (associated with long-term fluctuations) of the same order of magnitude ($\sim 10^{-3}$) were also suppressed. Thus, a high-quality A spectrum can be obtained quickly in a single measurement with balanced detection.

To fully realize the benefits of balanced detection, we found it necessary to sample I and I_{ref} (and I_0 and $I_{0,ref}$) in a multiplex manner. In multiplex sampling, a single analog-to-digital converter digitizes the analog signals.[21] While the n analog signals are sampled at the same rate, the n analog signals are digitized sequentially at a rate n times larger than the sampling rate. In this way, the noises associated with I and I_{ref} (and I_0 and $I_{0,ref}$) in A are similar. Appendix D shows that the noise amplitude (1×10^{-3}) is the same when I (I_0) and I_{ref} ($I_{0,ref}$) are sampled sequentially, even when balanced detection is implemented. In contrast, the noise is reduced to 3×10^{-4} when I (I_0) and I_{ref} ($I_{0,ref}$) are sampled in a multiplexed manner and balanced detection is implemented.

Figure 5 displays the A spectrum of Dy 754 measured at 77 K. Sharpening of the absorption bands is evident, as compared with the spectrum of Dy 754 measured at ~295 K (Fig. 4). The inset of Fig. 5 shows A spectra in a region where there is little or no signal, measured in a variety of configurations. A critical benchmark is when just the cryostat is in the beam path, without any liquid nitrogen or sample; in this case, the noise amplitude is 2×10^{-4}. The addition of liquid nitrogen doubled the noise amplitude to 4×10^{-4}. We attribute this relatively small increase in the noise amplitude to: (i) the use of a cryostat with a dual reservoir design,[11,22] which prevents the fluid in the beam path from boiling and suppresses schlieren effects, and (ii) filling the inner reservoir by condensing high-purity (99.999%) nitrogen gas, which minimizes scatter from ice and other contaminants/particulates. With a glycerol:buffer sample added, the noise amplitude again increased to 7×10^{-4}. In this case, noise may be added via imperfect glass formation (i.e., scatter) and from the presence of a series of interfaces (i.e., nitrogen, glass, conductor, sample, etc.). Critically, these measurements were undertaken without physically moving the sample between I and I_0 scans. Finally, measurements on a Dy 754 sample in the capacitor resulted in a noise amplitude of 1×10^{-3} when considering the entire spectral range; however, excluding obvious erroneous spikes from the analysis, the noise amplitude was 7×10^{-4}, which matched that of the experiment on the glycerol:buffer. Our current efforts aim to improve the quality of the glass to attain a noise amplitude matching that of the liquid nitrogen only in experiment, i.e., 4×10^{-4}. Nevertheless, the measured noise floor of 7×10^{-4} represents a significant improvement over the benchmark value of 1×10^{-2} suggested in prior work for absorption measurements,[5] which we attribute to a combination of improvements in the light source, cryogenics, and detection scheme.

To further evaluate the quality of the ΔA spectra obtained by the ESS, we measured ΔA spectra at a series of applied field strengths (Fig. 6). At the maximum field strength of ~400 kV/cm, the absolute amplitude of the most prominent signal at 735 nm was $\sim 7.3 \times 10^{-4}$, which, given a noise amplitude of 6×10^{-6}, corresponds to a S/N of ~122. For reference, noise amplitudes of this order of magnitude have been achieved in the literature,[4,10,23–27] although it is not clear as to what extent ensemble averaging contributed to the reduction of noise in these examples. A quadratic fit to a plot of the maximum signal amplitude as a function of applied field strength yields a coefficient of determination (i.e., R^2) of unity (data not shown), consistent with the expected quadratic field dependence of the observed signal.[8,11] At 50 kV/cm, the signal exhibits an amplitude of

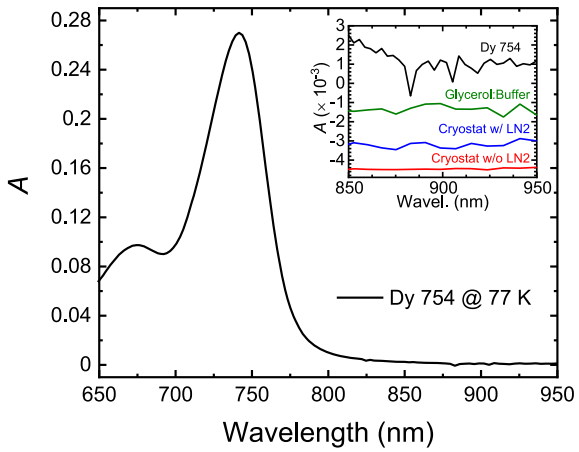

FIG. 5. A spectrum of a ~240 μM solution of Dy 754 dissolved in a glycerol:aqueous buffer solution contained in a ~55 μm spaced capacitor at 77 K. The inset displays four measurements in a region of the spectrum from 850 to 950 nm with little to no signal to aid comparison of the respective noise levels. The four measurements are for the cases where the dual-immersion cryostat was in the beam path: (i) without either liquid nitrogen or a sample in the chamber, (ii) with liquid nitrogen in the chamber but without any sample, (iii) with liquid nitrogen and a glycerol:buffer sample in the chamber, and (iv) with liquid nitrogen and a Dy 754 sample in the chamber.

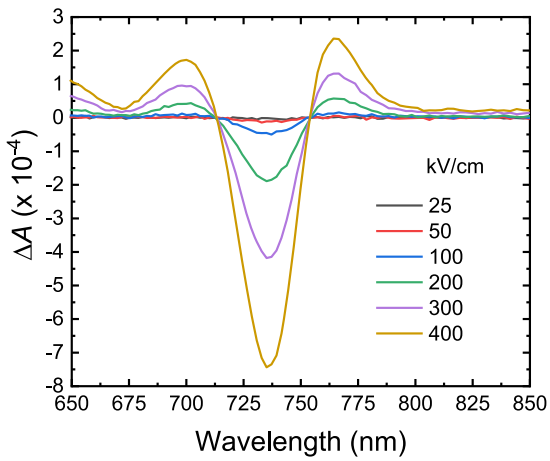

FIG. 6. ΔA ($= -\Delta I/I$) spectra as a function of applied field strength. The colors of the traces and corresponding field strength are indicated in the inset. The modulation frequency was 350 Hz, and the signal was detected at 700 Hz, i.e., twice the modulation frequency. Additional experimental details are included in the methods.

$\sim 1.2 \times 10^{-5}$, which corresponds to a S/N of 2 and is the minimum resolvable signal.[20] Thus, it was not possible to resolve the signal at 25 kV/cm, where, based on the quadratic dependence, we expect an amplitude of $\sim 3 \times 10^{-6}$ (and S/N of 0.5).

Finally, the ESS includes a monochromator that permits measurements with constant wavenumber (i.e., energy) bandpass, which presents an advantage in the Liptay analysis over alternative schemes that implement constant wavelength bandpass (by virtue of fixed or manually mechanically adjusted slit widths). In a constant wavelength bandpass measurement, for example, the spectral resolution in energy becomes poorer at shorter wavelengths due to the reciprocal relationship between wavelength and energy, possibly resulting in a loss in accuracy in both A and ΔA measurements. While we observed no distinguishable differences between ΔA spectra measured with constant wavelength and energy bandpass for Dy 754 (data not shown), differences may be observed for samples that exhibit finely spaced spectral features across a broad spectral window. One such example is dilute solutions of polycyclic aromatic hydrocarbons in Shpolskii matrices at cryogenic temperatures.[28] Another advantage of constant energy bandpass applies to absolute intensity measurements such as the fluorescence emission spectrum needed in Stark fluorescence characterization. While the intensities collected with constant wavelength bandpass must be nonlinearly scaled to correct for the inverse relationship between wavelength and energy,[29] no such correction is needed for spectra collected with constant energy bandpass.

There is still room for improvement. In a future implementations, we will use all-reflective optics, specifically off-axis parabolic mirrors, to reduce the optical aberrations induced by transmissive optics. In principle, we can focus the light to a spot as small as the size of the initial image (that is, the diameter of the xenon plasma in the LDLS), which is ~100–200 μm.[30] In preliminary work, we were able to focus the light to a spot of size ~300 μm, which is consistent with this expectation. Such a small spot size will facilitate avoiding imperfections of the sample glass (thereby potentially reducing noise arising from scattered light, as discussed above in the context of Fig. 5) and ensure the complete detection of the light, since the area of most high-sensitivity sensors is only ~1 mm^2.

IV. CONCLUSIONS

In conclusion, we have reported a high-sensitivity ESS that features an LDLS. The intensity fluctuations of the LDLS were characterized and compared with an arc-driven xenon lamp; the LDLS was found to exhibit comparable, though slightly better, performance. A detection scheme based on a combination of balanced detection and multiplex sampling was implemented to reduce noise in A. Noise amplitudes were low for both A and ΔA, comparable to or better than past literature precedents, which permitted high S/N measurements on concentrated solutions of a conjugated asymmetric polymethine molecule. This work will facilitate wider access to, and broader use of, this powerful spectroscopic method.

ACKNOWLEDGMENTS

Research at Boise State was supported wholly by the U.S. Department of Energy (DOE), Office of Basic Energy Sciences, Materials Sciences and Engineering Division, and DOE's Established Program to Stimulate Competitive Research (EPSCoR), under Award No. DE-SC0020089. C.J.V.G. and R.J.S. gratefully acknowledge partial support from the National Aeronautics and Space Administration's (NASA's) Exobiology program (Grant No. 80NSSC17K0033). J.S.H. and R.D.P. thank D. Logan and J. Dean for tips and feedback on cryogenics and J. Momberger for the same on vacuum systems; R.D.P. also thanks A. Loukianov for initial guidance on the ESS and D. Hahn for technical details on the monochromator.

AUTHOR DECLARATIONS

Conflict of Interest

The authors have no conflicts to disclose.

Author Contributions

Jonathan S. Huff: Data curation (equal); Investigation (equal); Methodology (equal); Software (equal); Writing – original draft (supporting); Writing – review & editing (supporting). **Katelyn M. Duncan**: Data curation (equal); Formal analysis (equal); Investigation (equal); Methodology (equal); Validation (equal); Writing – original draft (equal); Writing – review & editing (supporting). **Cornelius J. van Galen**: Investigation (supporting); Writing – review & editing (supporting). **Matthew S. Barclay**: Investigation (supporting). **William B. Knowlton**: Conceptualization (supporting); Funding acquisition (lead); Project administration (equal); Writing – review & editing (supporting). **Bernard Yurke**: Conceptualization (supporting); Funding acquisition (supporting); Writing – review & editing (supporting). **Paul H. Davis**: Investigation (supporting); Methodology (equal); Writing – review & editing (supporting). **Daniel B. Turner**: Formal analysis (equal); Funding acquisition (supporting); Investigation (equal); Methodology (equal); Supervision (equal); Writing – review & editing (equal). **Robert J. Stanley**: Conceptualization (supporting); Investigation (supporting); Writing – review & editing (supporting). **Ryan D. Pensack**: Conceptualization (lead); Data curation (equal); Formal analysis (equal); Funding acquisition (supporting); Investigation (equal); Methodology (equal); Project administration (equal); Software (equal); Supervision (lead); Validation (equal); Writing – original draft (equal); Writing – review & editing (lead).

DATA AVAILABILITY

The data that support the findings of this study are available from the corresponding author upon reasonable request.

APPENDIX A: LIGHT-SOURCE INTENSITY OSCILLATIONS AND ANALOG LOW-PASS FILTER

Figure 7 displays measurements of the LDLS intensity, with and without an analog low-pass 10 kHz filter, between PD2 and the terminal block transmitting the signals to the DAQ board. Without the filter, large oscillations (±0.6%) are observed, with a period of ~23.467 μs (corresponding to a plasma oscillation frequency of ~41.613 kHz), which is longer than the ~4.8 μs period (~210 kHz

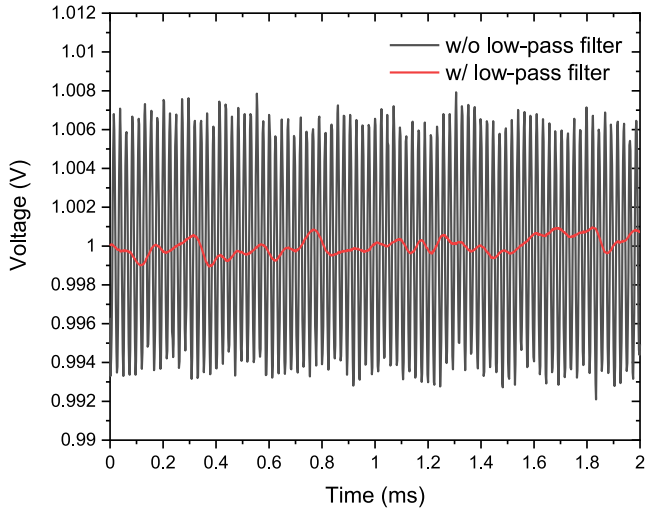

FIG. 7. Measurements of the LDLS intensity, with (red) and without (black) an analog low-pass 10 kHz filter. The signal was measured at PD2 with 850 nm light.

frequency) reported by Su and Lin.[18] With the filter, the oscillations are considerably reduced in amplitude.

APPENDIX B: DETECTION ELECTRONICS, TRIGGER SCHEME, AND HIGH-VOLTAGE ELECTRONICS

Figure 8 displays the detection electronics, trigger scheme, and high-voltage electronics, including the sample rod and components. For the high-voltage electronics, all parts, except for the high-voltage coaxial cable (Pasternack, RG8X), were purchased from McMaster-Carr.

The sample holder was 3D printed and is composed of polylactic acid. The capacitor consisted of the sample sandwiched between two pieces of boro-aluminosilicate glass coated with indium-tin oxide on one surface, which were 1.1 mm thick and had an area of 25 × 25 mm^2 (Delta Technologies, CB-40IN-0111). Four strips of 55 μm thick Kapton were placed between the two pieces of glass. The thickness of the Kapton was measured with a digital micrometer (Mitutoyo, 292-832-30).

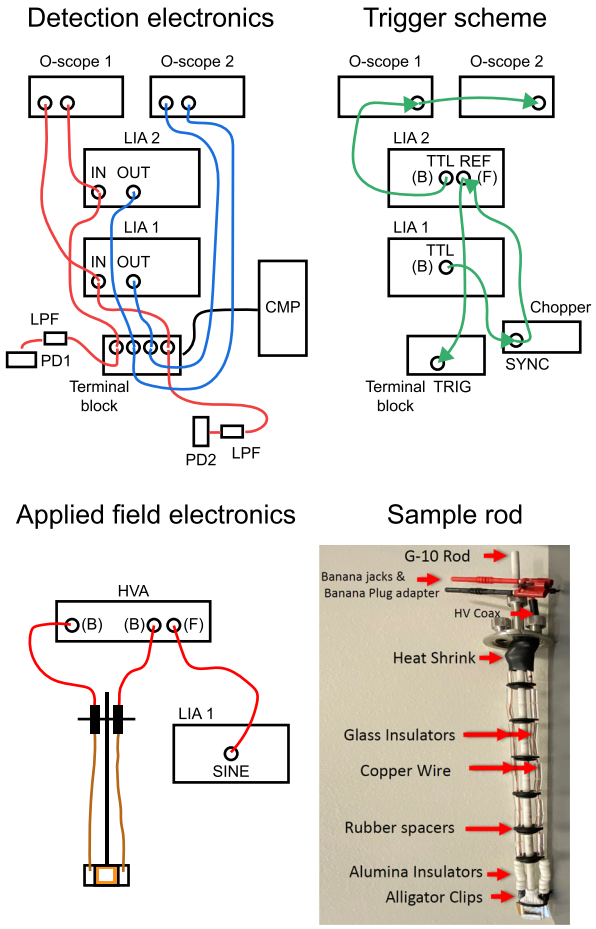

FIG. 8. (Top, left) Detection electronics. Red and blue lines depict BNC wires transmitting the photodiode and lock-in amplifier outputs, respectively. The black line depicts a shielded, 2-m-long multifunction cable, transmitting the terminal block output. (Top, right) Trigger scheme. Green lines depict BNC wires transmitting the LIA 1 output and 2 TTL outputs. The arrows at the end of the green lines depict the direction of signal propagation. The (B) and (F) labels indicate the back and front side of the panels of the equipment, respectively. (Bottom, left) Schematic of applied field electronics. (Bottom, right) Photo of sample rod and components. The sample capacitor is at the bottom of the photo.

APPENDIX C: ARC-DRIVEN XENON LAMP INTENSITY CHARACTERIZATION

To provide context for the observed LDLS intensity fluctuations, we characterized an arc-driven xenon lamp in an analogous manner. The arc-driven xenon lamp (Newport, 6259) was operated at ~300 W via a power supply (Newport 69911), which was regulated by a light intensity control system including a controller module (Newport, 68945) and thermoelectrically cooled silicon detector (Newport, 71582). The light was coupled to a spectrometer featuring an optical cryostat, which has been described in detail previously.[11] After the cryostat, the light was detected by a photodiode (OSI Optoelectronics, UDT455UV). The output signal was amplified by a custom-built amplifier, which was then digitized by a 16-bit DAQ board (National Instruments, PCI-6036). For the measurements below, the monochromator was set to transmit light at 850 nm.

Based on three sequential one-hour scans of the lamp intensity, the arc-driven lamp exhibited slightly higher RSD as compared with the LDLS. Specifically, the arc-driven lamp exhibited an RSD of 0.363 ± 0.005%. Additionally, the arc-driven lamp exhibited a drift of 0.2 ± 0.1%/h, which is about the same as that of the LDLS. The arc-driven lamp intensity fluctuations were also measured at a rate of 20 kHz, and an FFT was performed on the resulting data. The intensity fluctuations associated with the arc-driven lamp exhibited more $1/f$ and line noise as compared to that of the LDLS (Fig. 9). For the arc-driven lamp, the $1/f$ noise changes to white noise at frequencies above ~800 Hz, while this change appears at ~200 Hz for the LDLS. This result is consistent with the slightly higher RSD measured for

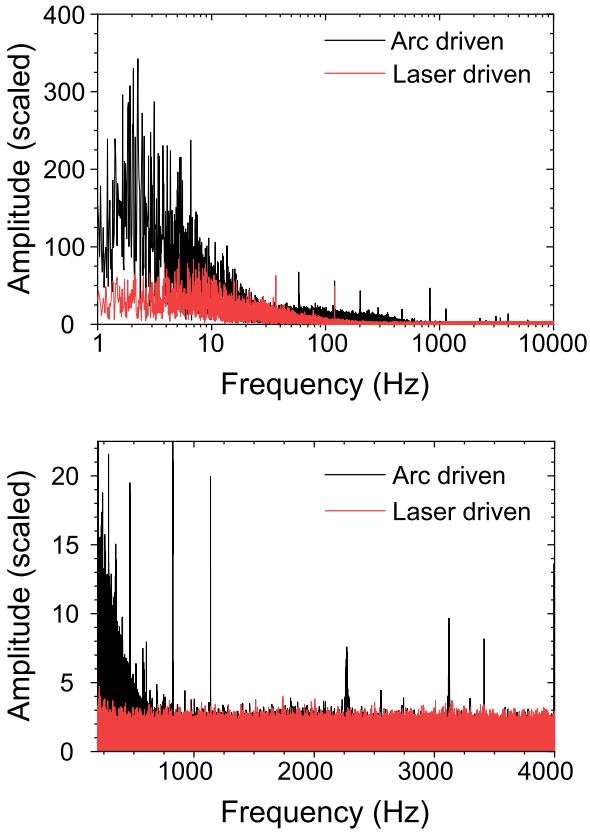

FIG. 9. Intensity fluctuations of an arc-driven xenon lamp (black trace) and LDLS (red trace), with the frequency axis plotted in a logarithmic (top) and linear (bottom) manner. Both datasets were scaled by dividing by the average amplitude from 1 to 3 kHz.

the arc-driven lamp. We, therefore, conclude that the LDLS exhibits intensity fluctuations that are comparable to or better than those associated with an arc-driven light source.

APPENDIX D: BALANCED DETECTION OF *A* AND SEQUENTIAL vs MULTIPLEX SAMPLING

Figure 10 displays A spectra for the cases where I and I_{ref} (and I_0 and $I_{0,ref}$) were sampled sequentially and in a multiplex manner, and where the spectra were calculated with and without balanced detection. Long-timescale drift is evident in both spectra, measured with sequential and multiplex sampling and calculated without balanced detection. Short-timescale fluctuations are characterized by the noise amplitude, i.e., the maximum point-by-point deviation. The noise amplitude was 1×10^{-3} in the case of sequential sampling, with and without balanced detection. Thus, although long-timescale drift was corrected, short-timescale fluctuations were not suppressed. In the case of multiplex sampling, the noise amplitude was 3×10^{-4} and 1×10^{-3}, with and without balanced detection, respectively. Thus, a combination of multiplex sampling and balanced detection is needed to suppress both long-timescale drift and short-timescale fluctuations.

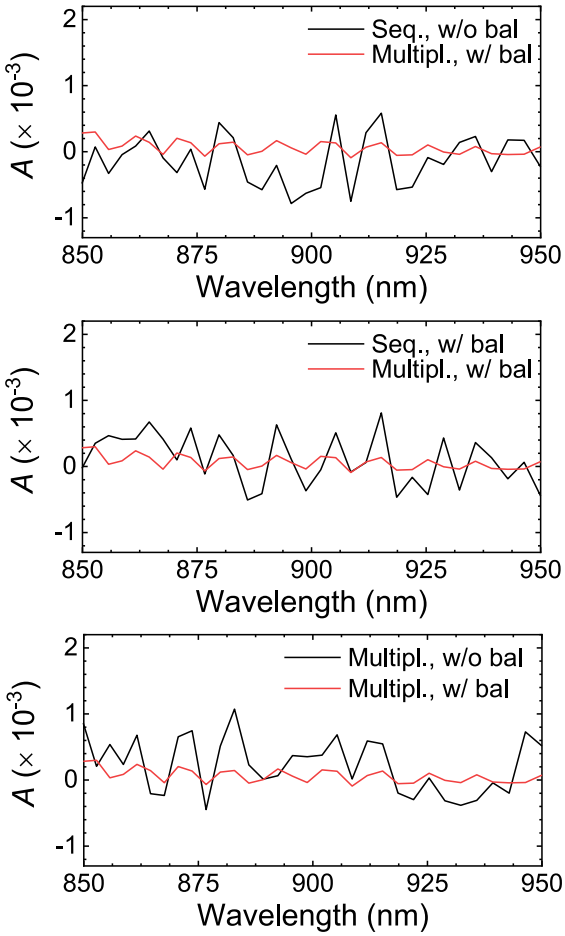

FIG. 10. Same data as in Fig. 4 inset showing the A measurements made using multiplex sampling with balanced detection (red trace) compared with: (top) sequential sampling without balanced detection, (middle) sequential sampling with balanced detection, and (bottom) multiplex sampling without balanced detection. These data were collected on an aqueous buffer solution of Dy 754 in a 2 mm path length cuvette. The time constant was 100 ms, and the chopping frequency was 1000 Hz.

REFERENCES

[1] D. J. Lockhart and S. G. Boxer, "Magnitude and direction of the change in dipole moment associated with excitation of the primary electron donor in Rhodopseudomonas sphaeroides reaction centers," Biochemistry **26**(3), 664–668 (1987).

[2] L. L. Premvardhan and L. A. Peteanu, "Dipolar properties of and temperature effects on the electronic states of 3-Hydroxyflavone (3HF) determined using Stark-effect spectroscopy and compared to electronic structure calculations," J. Phys. Chem. A **103**(37), 7506–7514 (1999).

[3] A. B. Maurer, E. J. Piechota, and G. J. Meyer, "Excited-state dipole moments of homoleptic $[Ru(bpy')_3]^{2+}$ complexes measured by Stark spectroscopy," J. Phys. Chem. A **123**(41), 8745–8754 (2019).

[4] C. van Galen, D. T. Barnard, and R. J. Stanley, "Stark spectroscopy of lumichrome: A possible candidate for stand-off detection of bacterial quorum sensing," J. Phys. Chem. B **124**(52), 11835–11842 (2020).

[5]G. U. Bublitz and S. G. Boxer, "STARK SPECTROSCOPY: Applications in chemistry, biology, and materials science," Annu. Rev. Phys. Chem. **48**(1), 213–242 (1997).
[6]F. W. Vance, R. D. Williams, and J. T. Hupp, "Electroabsorption spectroscopy of molecular inorganic compounds," Int. Rev. Phys. Chem. **17**(3), 307–329 (1998).
[7]R. J. Stanley, "Advances in flavin and flavoprotein optical spectroscopy," Antioxid. Redox Signaling **3**(5), 847–866 (2001).
[8]S. G. Boxer, "Stark Realities," J. Phys. Chem. B **113**(10), 2972–2983 (2009).
[9]S. G. Boxer, *Photosynthetic Reaction Center*, edited by J. Deisenhofer and J. R. Norris (Academic Press, San Diego, CA, 1993), pp. 179–220.
[10]R. F. Pauszek and R. J. Stanley, *Flavins and Flavoproteins: Methods and Protocols*, edited by S. Weber and E. Schleicher (Springer, New York, 2014), pp. 443–466.
[11]R. J. Stanley and C. J. van Galen, *Methods in Enzymology*, edited by B. A. Palfey (Academic Press, 2019), pp. 215–250.
[12]D. Redfield, "Arc lamp intensity stabilizer," Rev. Sci. Instrum. **32**(5), 557–558 (1961).
[13]W. Budde, "Stability of high-pressure xenon lamps," J. Opt. Soc. Am. **52**(3), 343–345 (1962).
[14]R. H. Breeze and B. Ke, "Some comments on xenon arc lamp stability," Rev. Sci. Instrum. **43**(5), 821–823 (1972).
[15]D. Smith, US20070228288A1 (4 October 2007).
[16]E. R. Kennehan, C. Grieco, A. N. Brigeman, G. S. Doucette, A. Rimshaw, K. Bisgaier, N. C. Giebink, and J. B. Asbury, "Using molecular vibrations to probe exciton delocalization in films of perylene diimides with ultrafast mid-IR spectroscopy," Phys. Chem. Chem. Phys. **19**(36), 24829–24839 (2017).
[17]D. de Sa Pereira, C. Menelaou, A. Danos, C. Marian, and A. P. Monkman, "Electroabsorption spectroscopy as a tool for probing charge transfer and state mixing in thermally activated delayed fluorescence emitters," J. Phys. Chem. Lett. **10**(12), 3205–3211 (2019).
[18]M.-N. Su and J. Jr-Min Lin, "Note: A transient absorption spectrometer using an ultra bright laser-driven light source," Rev. Sci. Instrum. **84**(8), 086106 (2013).
[19]N. V. Tkachenko, *Optical Spectroscopy: Methods and Instrumentations* (Elsevier, 2006).
[20]D. A. Skoog, F. J. Holler, and T. A. Nieman, *Principles of Instrumental Analysis*, 5th ed. (Brooks Cole, 1997).
[21]National Instruments and NI-DAQmx, NI-DAQmx Help (2022).
[22]S. S. Andrews and S. G. Boxer, "A liquid nitrogen immersion cryostat for optical measurements," Rev. Sci. Instrum. **71**(9), 3567–3569 (2000).
[23]D. H. Oh and S. G. Boxer, "Electrochromism in the near-infrared absorption spectra of bridged ruthenium mixed-valence complexes," J. Am. Chem. Soc. **112**(22), 8161–8162 (1990).
[24]D. S. Gottfried, M. A. Steffen, and S. G. Boxer, "Large protein-induced dipoles for a symmetric carotenoid in a photosynthetic antenna complex," Science **251**(4994), 662–665 (1991).
[25]M. Liess, S. Jeglinski, Z. V. Vardeny, M. Ozaki, K. Yoshino, Y. Ding, and T. Barton, "Electroabsorption spectroscopy of luminescent and nonluminescent π-conjugated polymers," Phys. Rev. B **56**(24), 15712–15724 (1997).
[26]J. Tayama, T. Iimori, and N. Ohta, "Comparative study of electroabsorption spectra of polar and nonpolar organic molecules in solution and in a polymer film," J. Chem. Phys. **131**(24), 244509 (2009).
[27]A. Islam, Y. Kikuchi, and T. Iimori, "Electroabsorption and Stark fluorescence spectroscopies of Thioflavin T," J. Phys. Chem. A **127**(6), 1436–1444 (2023).
[28]L. A. Nakhimovsky, M. Lamotte, and J. Joussot-Dubien, *Handbook of Low Temperature Electronic Spectra of Polycyclic Aromatic Hydrocarbons* (Elsevier, 1989).
[29]J. Mooney and P. Kambhampati, "Get the basics right: Jacobian conversion of wavelength and energy scales for quantitative analysis of emission spectra," J. Phys. Chem. Lett. **4**(19), 3316–3318 (2013).
[30]M. Steinberg, "Application spot light: Laser-driven light sources for ellipsometry," Energetiq Application Note #001-10-2020 (2020).